PCCP

Theoretical design of durable and strong polycarbonate against photodegradation

Journal:	*Physical Chemistry Chemical Physics*
Manuscript ID	CP-COM-07-2023-003533.R1
Article Type:	Communication
Date Submitted by the Author:	24-Nov-2023

Complete List of Authors:	Huang, Xiao; Kyushu University, Department of Interdisciplinary Engineering Sciences Orimoto, Yuuichi; Kyushu University, Department of Advanced Materials Science and Engineering, Faculty of Engineering Sciences Aoki, Yuriko; Kyushu University, Faculty of Engineering Sciences, Department of Material Sciences

COMMUNICATION

Theoretical design of durable and strong polycarbonate against photodegradation

Received 00th January 20xx,
Accepted 00th January 20xx

DOI: 10.1039/x0xx00000x

Xiao Huang,[a] Yuuichi Orimoto[b] and Yuriko Aoki[b,*]

The photodegradation mechanism of polycarbonate (PC) was investigated by quantum chemistry, and a novel antidegradation molecular design using substituents was proposed. It was demonstrated that electron-withdrawing substituents in the phenyl moiety control the bond alternation, leading to inhibition of the O–C bond cleavage in the carbonate moiety. This result may provide a promising alternative for durable PC synthesis.

Bisphenol-A polycarbonate (BPA PC) is a widely used material in our daily life due to its good transparency, high toughness, and other good performances[1]. It will lose the physical properties notably if overexposed to sunlight or ultraviolet (UV) light.[2,3] To improve the PC performance, a common strategy in experiment[4-12] is to modify the PC chemical structure. Among them, replacing PC phenyl hydrogen atoms by electron-donating or -withdrawing groups would make it possible to reach the above goal by suppressing PC photodegradation.

A few computational mechanistic studies were focused on photodegradation of PC[13] and aromatic esters[14,15]. Recently, our group reported the mechanism of PhO–COO bond scission using a simplified PC model bisphenol-A hydrogen carbonate (BPAHC, Fig. 1) based on quantum chemical methods.[13] As shown in Fig. 1, two transitions are included in explaining O–C cleavage: $n_{(O\ of\ CO3)}\rightarrow\pi^*_{(Phenyl)}$ and $n_{(O\ of\ CO3)}\rightarrow\pi^*_{(CO3)}$. The former leads to the C–C extensions by strengthening C–C out-of-phase overlap within phenyl group and enhances the two C=C double bonds by C–C in-phase overlap. The two C=C bonds induce the Ph=O double bond due to geometric constraints, facilitating a quinoid-like structure formation, then breaking the PhO–COO bond. The latter further enhances the

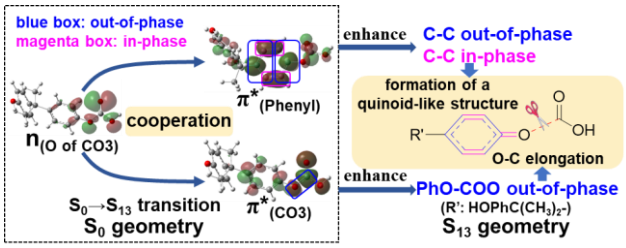

Fig. 1 The PhO–COO bond cleavage of BPAHC.

PhO–COO elongation by the reinforced out-of-phase overlap. These two transitions based on the ground state (GS) S_0 geometry jointly cleave the PhO–COO bond in the excited state (ES) S_{13} geometry.

Given the lack of theoretical studies on photodegradation of PC, our aim is to provide a detailed investigation of mechanism affected by substituents, expecting to design light-resistant PC materials. Therefore, based on our previous study[13], we applied density functional theory (DFT) and time-dependent DFT (TDDFT[16]) methods to study the substituent effect on the photodegradation of two PC models with electron-donating (-NH_2) and -withdrawing (-NO_2) groups as phenyl substituents.

The GSs and ESs geometries of *m*(NH_2)-BPAHC and *m*(NO_2)-BPAHC (Fig. 2) were fully optimized using B3LYP[17-19]/6-31G(d) and TD-B3LYP/6-31G(d), respectively, because B3LYP can generate the reasonable results (Figs. S1-S5 and Tables S1-S3) for these organic systems[20-22]. S_0 and S_n geometries in this study are the optimized geometries of the singlet GS and singlet n^{th} ES, respectively. Computational details were in ESI†.

To assess the substituent effect on the carbonate O–C bond, Fig. 3 shows the transition behaviors of the studied models. As

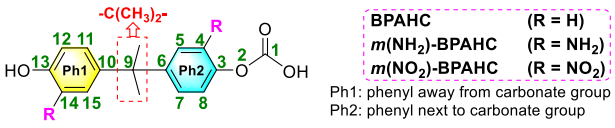

Fig. 2 Molecular structures of BPAHC and substituted BPAHC at -$C(CH_3)_2$- *meta*-positions (denoted as *m*(R)-BPAHC, R=NH_2, NO_2). (Bold green: atomic numbering)

[a] Department of Interdisciplinary Engineering Sciences, Chemistry and Materials Science, Interdisciplinary Graduate School of Engineering Sciences, Kyushu University, 6-1 Kasuga Park, Fukuoka 816-8580, Japan.
[b] Department of Material Sciences, Faculty of Engineering Sciences, Kyushu University, 6-1 Kasuga Park, Fukuoka 816-8580, Japan.
*E-mail: aoki.yuriko.397@m.kyushu-u.ac.jp.

† Footnotes relating to the title and/or authors should appear here.
Electronic Supplementary Information (ESI) available: [details of any supplementary information available should be included here]. See DOI: 10.1039/x0xx00000x

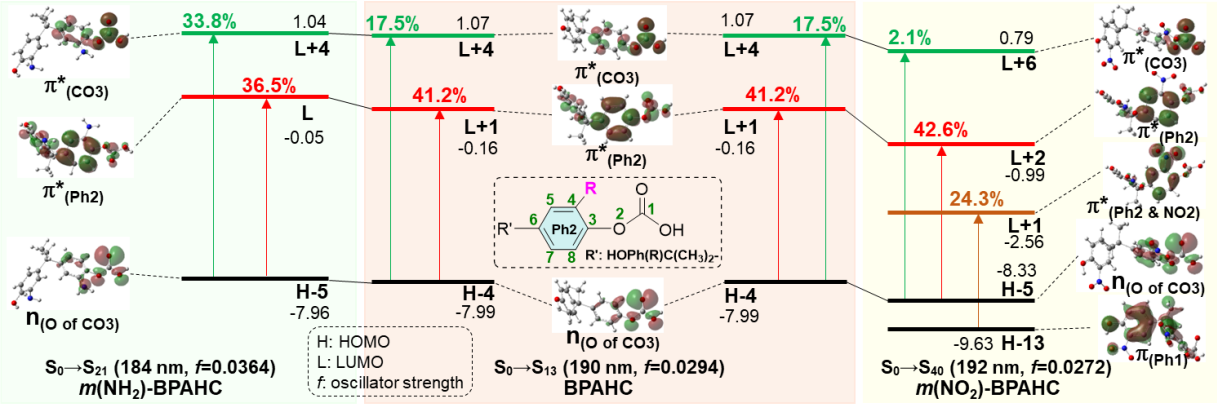

Fig. 3 Calculated molecular orbitals (MOs) (isovalue=0.03) involved in vertical excitation of BPAHC, *m*(NH_2)-BPAHC, and *m*(NO_2)-BPAHC in S_0 geometry. (Percentage values: transition contribution. Black colored values: orbital energy in eV.)

reported in our previous study on BPAHC[13], the electronic transition (corresponding to $S_0 \rightarrow S_{13}$ excitation in the current study) contributed by $n_{(O\ of\ CO3)} \rightarrow \pi^*_{(Ph2)}$ and $n_{(O\ of\ CO3)} \rightarrow \pi^*_{(CO3)}$ plays a key role in breaking PhO–COO bond. Hence, $S_0 \rightarrow S_{21}$ (*m*(NH_2)-BPAHC) and $S_0 \rightarrow S_{40}$ (*m*(NO_2)-BPAHC) transitions are discussed because their major contributions also focus on the excitations to $\pi^*_{(Ph2)}$ and $\pi^*_{(CO3)}$ as in $S_0 \rightarrow S_{13}$ transition (Fig. 3). Relative to the oscillator strength of 0.0294 in $S_0 \rightarrow S_{13}$ transition, $S_0 \rightarrow S_{21}$ and $S_0 \rightarrow S_{40}$ transitions have similar values of 0.0364 and 0.0272, respectively, implying the similar impact on the absorption spectra. The absorption spectra and parameters of vertical excitation are shown in Fig. S6 and Table S4, respectively.

We start the discussion of the substituent effect on the O–C bond by examining the variation in transition contributions compared to BPAHC. In Fig. 3 left, the maintained large $n_{(O\ of\ CO3)} \rightarrow \pi^*_{(Ph2)}$ contribution (41.2→36.5%) and the remarkable increased $n_{(O\ of\ CO3)} \rightarrow \pi^*_{(CO3)}$ contribution (17.5→33.8%) indicate the promotion of O2–C1 bond scission under the -NH_2 effect. In Fig. 3 right, the contributions excited to Ph2 π* orbitals remain substantial (41.2→42.6%), while that excited to $\pi^*_{(CO3)}$ orbital is nearly eliminated (17.5→2.1%), implying the suppression of O2–C1 bond cleavage influenced by -NO_2 group.

To further examine the substituent impact on the O–C bond, Fig. 4 and Fig. S7 show the GS and ES geometries of the studied models. By excitation, S_{13} geometry (Fig. 4 center) of BPAHC with a distorted Ph2 group relative to S_0 geometry is prone to be a quinoid-like structure along C6-C3-O2 line with C4=C5, C7=C8, and C3=O2 bonds, finally cleaving the O2–C1 bond.

Similarly, by excitation of $n_{(O\ of\ CO3)} \rightarrow \pi^*_{(Ph2)}$, S_{21} geometry (Fig. 4 top) of *m*(NH_2)-BPAHC tends to be a different quinoid-like structure with C4=C5, C6=C7, and C3=O2 bonds from that of BPAHC. It might come from the reason that in-phase interaction on C7=C8 in BPAHC is destroyed on C7–C8 at L ($\pi^*_{(Ph2)}$) orbital due to the phase-node along C7-C4-NH_2 line (Fig. 3 left) in *m*(NH_2)-BPAHC. The maintained C4–NH_2 single bond nature in S_{21} geometry relative to S_0 geometry enables the bond alternation along O2-C3-C4-C5 line, leading to C3=O2 double bond nature, finally breaking the O2–C1 bond, which is the same behavior as in S_{13} geometry of BPAHC[13].

Distinct from the result of BPAHC[13], for *m*(NO_2)-BPAHC in Fig. 4 bottom, the O2–C1 bond remains a single bond nature in S_{40} geometry as in S_0 geometry, implying it is not easy to be broken by excitation under the -NO_2 effect. The C4–NO_2 bond (1.362 Å) of S_{40} geometry is much shorter than that (1.472 Å) of S_0 geometry, revealing the C4=NO_2 bond formation in S_{40} geometry. Relative to S_{13} geometry of BPAHC, S_{40} geometry tends to be a new quinoid-like structure with C3=C8, C5=C6, and C4=NO_2 bonds upon excitation. It can be considered that the in-phase interaction on C7=C8 in BPAHC is destroyed on C7–C8 at L+2 ($\pi^*_{(Ph2)}$) orbital due to -NO_2 substitution (Fig. 3 right) as in *m*(NH_2)-BPAHC. The C4=NO_2 bond formation allows the bond alternation along C7-C4-NO_2 line, keeping C3–O2 single bond nature, finally suppressing the O2–C1 bond scission. For ES geometry of *m*(NO_2)-BPAHC, there may be another possible alternated structure with C3=O2 and C7=C8 bonds that was not obtained via calculation (Fig. S8). However, such an ES structure like S_{40} geometry may not exist in BPAHC and *m*(NH_2)-BPAHC. Because in BPAHC no substituent locates at -$C(CH_3)_2$- *meta*-positions, and in *m*(NH_2)-BPAHC the C4–NH_2 bond keeps the single bond nature in S_{21} geometry. To exclude the possibility of such ES structure in *m*(NO_2)-BPAHC, Fig. S9 shows the geometric comparisons from different starting structures S_0' and S_0''. The results show this ES structure is not favored even from different starting structures.

To explore the substituent influence on the above geometric changes, Fig. 5 displays the MO comparisons in S_0 geometry for

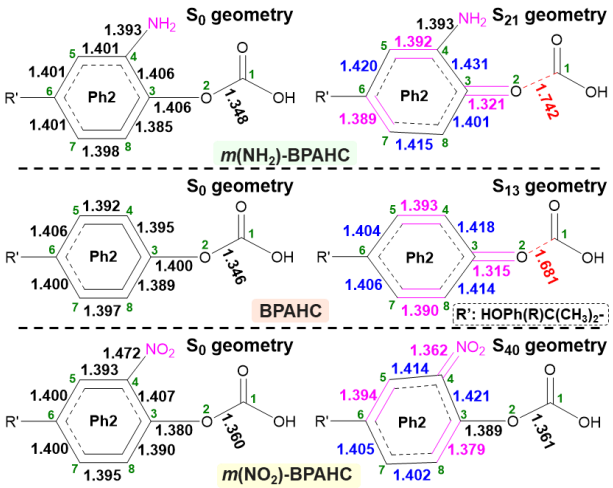

Fig. 4 GS and ES geometries of BPAHC, *m*(NH_2)-BPAHC, and *m*(NO_2)-BPAHC including main bond lengths (Å).

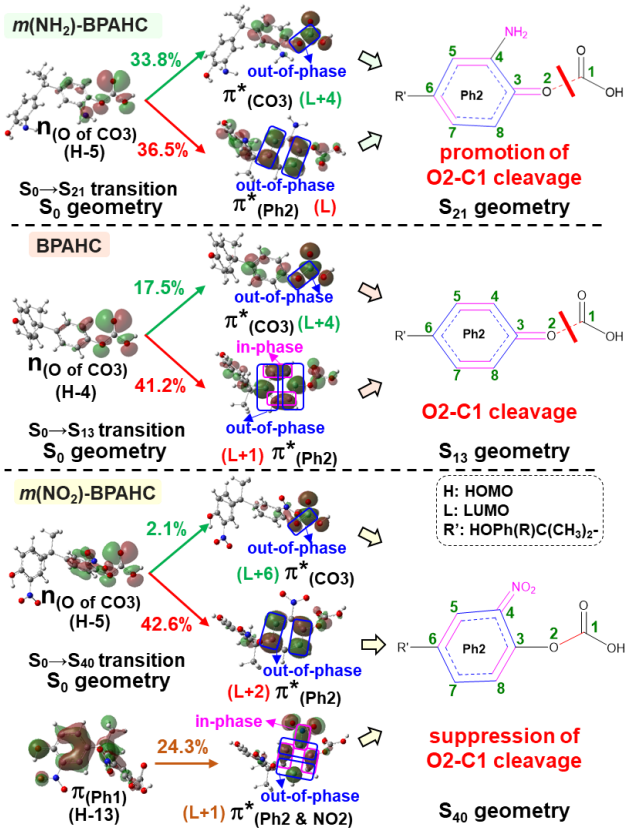

Fig. 5 The transitions of BPAHC, *m*(NH_2)-BPAHC, and *m*(NO_2)-BPAHC in S_0 geometry, and the corresponding ES geometries. (Percentage values: transition contribution.)

the studied models. For BPAHC in Fig. 5 center, by excitation to $\pi^*_{(Ph2)}$, the C3–C4, C3–C8, C5–C6, and C6–C7 bonds are elongated by enhancing out-of-phase overlaps (blue boxes of $\pi^*_{(Ph2)}$). These C–C elongations lead to a distorted Ph2 in S_{13} geometry relative to S_0 geometry, having the in-phase C4=C5 and C7=C8 bonds enhanced by C–C in-phase overlaps (magenta boxes of $\pi^*_{(Ph2)}$), forming a quinoid-like structure in S_{13} geometry. Upon excitation to $\pi^*_{(CO3)}$, the reinforced O2–C1 out-of-phase overlap (blue box of $\pi^*_{(CO3)}$) results in the O2–C1 bond elongation. These two excitations cause the O2-C1 bond breakage in S13 geometry.

In *m*(NH_2)-BPAHC, the O2–C1 bond cleavage in S_{21} geometry compared to S_0 geometry occurs as in BPAHC. In Fig. 5 top, the C3–C8 and C5–C6 bonds are stretched due to the enhanced out-of-phase overlaps (blue boxes of $\pi^*_{(Ph2)}$) upon excitation to $\pi^*_{(Ph2)}$. These two C–C extensions result in a distorted Ph2 group in S_{21} geometry relative to S_0 geometry, forming the C4=C5 and C6=C7 bonds due to geometric constraints. Hence, another quinoid-like structure different from that of BPAHC is formed in S_{21} geometry, breaking the O2–C1 bond. By excitation to $\pi^*_{(CO3)}$, the O2–C1 extension occurs because of the enhanced out-of-phase overlap (blue box of $\pi^*_{(CO3)}$). These two transitions cause the O2–C1 bond scission in S_{21} geometry as in BPAHC. Besides, a stronger driving force exists to elongate the O2–C1 bond, due to a higher transition contribution in *m*(NH_2)-BPAHC by excitation to $\pi^*_{(CO3)}$ (33.8%) relative to that of BPAHC (17.5%), implying that -NH_2 group can promote O2–C1 bond scission.

Conversely, in *m*(NO_2)-BPAHC, the O2–C1 bond keeps a single bond nature in S_{40} geometry as in S_0 geometry. There are two factors from Fig. 5 bottom: (1) the enhanced C4–NO_2 in-phase overlap (magenta box of $\pi^*_{(Ph2\ \&\ NO2)}$), and (2) the out-of-phase overlap at C3–C8 and C5–C6 (blue boxes of $\pi^*_{(Ph2\ and\ NO2)}$). The former leads to much shorter C4=NO_2 formation as well as shorter C3–C8 and C5–C6, while the latter to be longer in all lengths between carbons in phenyl ring. (2) has a larger weight than (1) by excited states calculations. Nevertheless, (2)'s effect doesn't appear in excited geometries. From the two factors of (1) and (2), it is suggested that the resulting C3=C8 and C5=C6 imply a very strong geometric effect of bond alternation caused by (1) C4=NO_2 compared to the out-of-phase effect in (2). Finally, a new quinoid-like structure of S_{40} geometry along C7-C4–NO_2 line is formed strongly affected by very short C4=NO_2, suppressing the O2–C1 bond cleavage under the -NO_2 effect.

To analyze the O–C bond scission affected by substituents, Fig. 6 shows the potential energy surfaces (PESs) by scanning the O2–C1 bond length and C4-C3-O2-C1 dihedral angle for the studied models, and Figs. S10-S12 display the other three views of PESs. In Fig. 6 center and Fig. S10, points **f1**, **e1**, and **g1** correspond to the local minimums on S_{13} PES of BPAHC[13]. Point **f1** corresponds to S_{13} geometry where the O2–C1 bond is broken. It has a lower energy of about 2.9 kcal/mol relative to point **b1** (the ES state via a vertical excitation from **a1** (S_0 geometry)). The energy barrier (**a1**→**f1**) for breaking the O2–C1

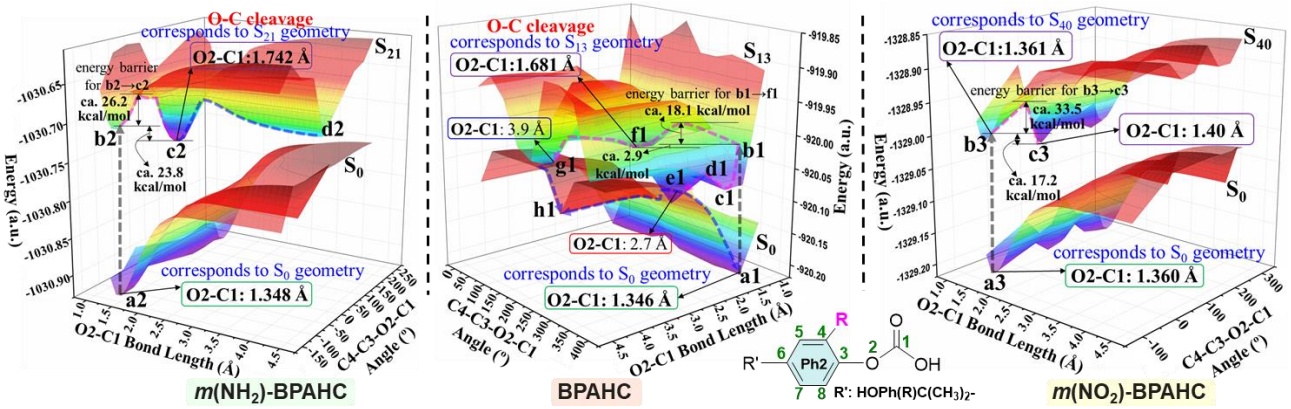

Fig. 6 PESs of GS and ES states for BPAHC, *m*(NH_2)-BPAHC, and *m*(NO_2)-BPAHC as the function of O2–C1 bond lengths and C4-C3-O2-C1 dihedral angles.

bond is about 18.1 kcal/mol, implying that it is easy to overcome this barrier to break the O2–C1 bond. Points **e1** and **g1** are the intersections between S_0 and S_{13} PESs, and the recombination (**e1**→**a1**) or separation (**e1**→**h1** or **g1**→**h1**) of the two radicals (Ph=O• and •COOH) may occur on S_0 PES from these two points. Besides, a possible intersystem crossing exists from the excited singlet to triplet via a crossing point (Fig. S13).

On PESs of *m*(NH_2)-BPAHC in Fig. 6 left and Fig. S11, the O2–C1 bond lengths at points **a2** and **c2** are 1.348 Å at S_0 geometry and 1.742 Å at S_{21} geometry, respectively. The O2–C1 bond is cleaved on S_{21} PES with an energy barrier of about 26.2 kcal/mol (**b2**→**c2**) that is a little higher than that in BPAHC. It is difficult to judge the substituent effect on the O2–C1 bond scission from this barrier via current coarse grid calculation. Relative to point **f1** energy (-2.9 kcal/mol) of BPAHC, energy of local minimum point **c2** is much lower by 23.8 kcal/mol than point **b2**, revealing that it is more likely to reach point **c2**. Differ from the PES result of BPAHC, there is no intersection between S_0 and S_{21} PESs in the current calculation, implying that recombining the broken O2····C1 pathway is blocked to some extent and the O2–C1 bond is easier to be cleaved. It indicates that -NH_2 group can promote the O2–C1 bond scission due to much lower energy of the local minimum point **c2** than that of BPAHC and the blockade to some degree of the damaged O2····C1 bond recombination.

For *m*(NO_2)-BPAHC in Fig. 6 right and Fig. S12, points **a3** and **b3** correspond to S_0 and S_{40} geometries, respectively. Unlike that of BPAHC, the O2–C1 bond cleavage does not occur in *m*(NO_2)-BPAHC because the O2–C1 bond lengths are similar in S_0 (1.360 Å) and S_{40} (1.361 Å) geometries. On S_{40} PES, a local minimum point **c3** has a lower energy of 17.2 kcal/mol relative to point **b3**. The energy barrier (**b3**→**c3**) is about 33.5 kcal/mol which is much higher than that of BPAHC, indicating that it is difficult to overcome this barrier to reach point **c3**. Besides, relative to BPAHC, the broken O2····C1 bond is difficult to recombine as there is no intersection between S_0 and S_{40} PESs. Hence, point **b3** may be a better location than **c3** (still 1.40 Å) on S_{40} PES, keeping O2–C1 single bond nature. It indicates that -NO_2 on phenyl rings can suppress the O2–C1 bond breakage.

In a word, the excitation to phenyl π* orbital is responsible for forming the quinoid-like structure, and to carbonate π* orbital is in charge of extending the carbonate O–C bond. These two excitations conjointly cleave the O–C bond in ES geometry. Relative to the result of BPAHC, the maintained high $n_{(O\ of\ CO3)}\rightarrow\pi^*_{(Ph2)}$ transition facilitates a quinoid-like structure formation with Ph=O bond, and the enhanced $n_{(O\ of\ CO3)}\rightarrow\pi^*_{(CO3)}$ transition facilitates the O–C bond extension, finally promoting the O–C bond cleavage in *m*(NH_2)-BPAHC. This promotion is further confirmed as the broken O····C bond recombination is somewhat hindered due to no intersection between GS and ES PESs. The S_{40} geometry with the O–C single bond nature is hard to overcome the much higher energy barrier than that of BPAHC, and the energy minimum at S_{40} energy surface is still short, keeping a bonding with 1.40 Å. Even if it's broken, the O····C bond is difficult to recombine due to the separation between S_0 and S_{40} PESs. These results can provide a comprehensive awareness and feasible direction of the UV-resistant PC material designs.

This work was financially supported by a Grant-in-Aid for JSPS Fellows DC1 (KAKENHI: 202321990) from Japan Society for the Promotion of Science (JSPS), and the Ministry of Education, Culture, Sports, Science and Technology of Japan (MEXT) (KAKENHI: JP23245005, JP16KT0059, JP25810103, JP15KT0146, JP16K08321, and JP20H00588), and the Japan Science and Technology Agency (JST), CREST. The computations were carried out by Linux systems in our research group and the high-performance computing systems at the Research Institute for Information Technology at Kyushu University.

Conflicts of interest

There are no conflicts to declare.

References

1 A. Rivaton, *Polym. Degrad. Stabil.*, 1995, **49**, 163-179.
2 A. Ram, O. Zilber and S. Kenig, *Polym. Eng. Sci.*, 1985, **25**, 535-540.
3 H. Liu, M. Zhou, Y. Zhou, S. Wang, G. Li, L. Jiang and Y. Dan, *Polym. Degrad. Stabil.*, 2014, **105**, 218-236.
4 A. Factor, M. L. Chu, *Polym. Degrad. Stabil.* 1980, **2**, 203-223.
5 A. Factor, W. V. Ligon and R. J. May, *Macromol.*, 1987, **20**, 2461-2468.
6 D. -J. Liaw, P. Chang, *Journal of Polymer Science: Part A: Polymer Chemistry.*, 1997, **35**, 2453-2460.
7 A. Factor, P. T. Engen, *Journal of Polymer Science: Part A: Polymer Chemistry.*, 1993, **31**, 2231-2236.
8 A. Factor, J. C. Lynch, *Journal of Polymer Science: Part A: Polymer Chemistry.*, 1987, **25**, 3413-3422.
9 A. Rivaton, J. Lemaire, *Polym. Degrad. Stabil.* 1988, **23**, 51-73.
10 G. M. Coppinger, E. R. Bell, *The Journal of Physical Chemistry*, 1966, **70**, 3479-3489.
11 D. -J. Liaw, P. Chang, *Polymer.* 1996, **37**, 2857-2863.
12 A. Rivaton, B. Mailhot, J. Soulestin, H. Varghese and J.-L. Gardette, *European Polymer Journal,* 2002, **38**, 1349-1363.
13 X. Huang, Y. Orimoto and Y. Aoki, *J. Phys. Chem. A*, 2021, **125**, 6662-6673.
14 S. Grimme, *Chem. Phys.*, 1992, **163**, 313-330.
15 J. M. Toldo, M. Barbatti and P. F. B. Gonçalves, *Phys. Chem. Chem. Phys.*, 2017, **19**, 19103-19108.
16 E. K. U. Gross, W. Kohn, *Adv. Quantum Chem.*, 1990, **21**, 255-291.
17 C. Lee, W. Yang and R. G. Parr, *Phys. Rev. B: Condens. Matter Mater. Phys.*, 1988, **37**, 785-789.
18 B. Miehlich, A. Savin, H. Stoll, H. Preuss, *Chem. Phys. Lett.*, 1989, **157**, 200-206.
19 A. D. Becke, *J. Chem. Phys.*, 1993, **98**, 5648-5652.
20 Y. Orimoto, K. Ishimoto and Y. Aoki, *J. Phys. Chem. C*, 2018, **122**, 4546-4556.
21 J. Xu, A. Takai, Y. Kobayashi and M. Takeuchi, *Chem. Commun.*, 2013, **49**, 8447-8449.
22 A. Francés-Monerris, M. Lineros-Rosa, M. A. Miranda, V. Lhiaubet-Vallet and A. Monari, *Chem. Commun.*, 2020, **56**, 4404-4407.